Evaluation of Range Extender Drive Train Topologies for Electric Vehicles

U.-J. Seo, J. Karthaus, K. Hameyer,
RWTH Aachen University,
Institute of Electrical Machines (IEM);

M. Böhmer, RWTH Aachen University,
Institute for Combustion Engines (VKA);

J. Schröter, RWTH Aachen University,
Institute for Machine Elements and Machine Design (IME)

Kurzfassung

Dieser Beitrag vergleicht vier unterschiedliche Range-Extender(REX)-Topologien für Elektrofahrzeuge. Der REX, bestehend aus Verbrennungsmotor und Generator, stellt zusätzliche Leistung im Falle einer Batterieerschöpfung bereit, um die Fahrdistanz zu erhöhen. Zwei verschiedene Verbrennungsmotoren und Generatoren sowie ein Getriebe werden miteinander verglichen. Drei Artemis-Fahrzyklen werden für eine Simulation des Batterie-Ladezustands verwendet. Die Fahrkosten werden anschließend mittels Wahrscheinlichkeitsverteilung der täglichen Fahrstrecke berechnet. Der Vergleich basiert auf Generator- und Fahrkosten, die aus der Simulation der Fahrzyklen entnommen werden.

Abstract

This paper compares four different range extender (REX) topologies for an electric vehicle (EV). In the REX-EV, the combustion engine and generator system provide alternative power to drive further after depleting battery energy. Two different combustion engines and generators as well as one transmission are employed for comparison. Three Artemis driving cycles are used for simulation of the charge sustaining mode. The driving costs can be calculated by the probability distribution of the daily driving distance. The comparison is based on the generator system costs and driving costs for a given result of driving cycle simulation.

1. Introduction

As the battery capacity of an electric vehicle is limited by various factors such as costs, weight and space, conventional vehicles with combustion engines still share the highest percentage on the vehicle market. To overcome the major drawback of the electric vehicle's

(EV) limited riving range, the use of range extender (REX) modules is a viable and promising alternative In the near term.

Table 1: REX-EV simulation parameters.

Vehicle mass	1480 kg
Rolling resistance	0.015
Aerodynamic coefficient	0.35
Battery Capacity	15 kWh
Engine power	30 kW
Motor power	80 kW

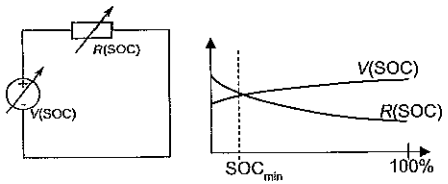

Figure 1: Battery equivalent circuit in this paper.

The REX concept in this paper is an auxiliary power source composed of an internal combustion engine (ICE) and a generator to increase the driving distance after depleting most of the battery's capacity. At the moment, previous studies of the REX application feature a direct driven [1,2] or a single stage gear driven [3,4] synchronous generator with relatively small gear ratio. The purpose of the transmission is to match the moved operating points via a gear stage to the engine's optimal operating point with the best efficiency region of the generator. This paper considers a high speed generator with a single stage transmission. Two 1.0 l gasoline engines with 30 kW, 29 kW respectively are employed. For each engine, two different 30 kW permanent magnet synchronous generators are used to compare the efficiency maps and to get indications of weight and costs. The surrogate model built by experimental results of the transmission is used for the efficiency of the transmission. The differences in driving costs for each topology is calculated based on the results of the driving cycle simulations. This paper concludes the comparative study of four different topologies using numerically and experimentally calculated models.

2. Modeling of the REX drive train concepts

The characteristics given in Table 1 are used to compare the REX topologies. The power

delivered to the electrical motor is the combined power of REX and battery:

$$P_d + P_{aux} = P_b + P_e, \quad (1)$$

where the subscripts d, aux, b and e are the demand of a driver, auxiliary demand, battery output and REX output power respectively. The model of each REX was built based on combined efficiency of the engine, transmission and generators. Below, this section introduces the details of each component.

A. Battery modeling

The Rint model, which neglects temperature effects, is adopted to represent a battery as shown in Fig. 1. The electrical circuit in the Rint model consists of a voltage source and a charging or discharging resistance which are function of the state of charge (SOC):

$$P_b = V_{oc} I_b - I_b^2 R_b, \quad (2)$$

$$I_b = \frac{V_{oc} \pm \sqrt{V_{oc}^2 - 4 I_b R_b}}{2R_b}, \quad (3)$$

$$V_{oc} = V(\mathrm{SOC}), \quad (4)$$

$$R_b = R_{dis}(\mathrm{SOC}) \text{ or } R_b = R_{ch}(\mathrm{SOC}). \quad (5)$$

The variation of SOC per a second due to consumed energy can be calculated as follows:

$$\Delta \mathrm{SOC} = \frac{-I_b}{Ah \cdot 3600}, \quad (6)$$

where *Ah* is the capacity of a fully charged battery in ampere hours and positive battery current is the discharged current of the battery.

B. Engine

The employed engines are naturally aspirated (NA) 1.0 l gasoline engines with port fuel injection (PFI). In comparison to the baseline engine, the advanced engine features an increased compression ratio, an integrated exhaust manifold, external exhaust gas recirculation (EGR) and reduced friction. These measures reduce specific fuel consumption almost in the entire engine map. The only drawback is the slightly reduced peak power for stoichiometric operation due to the higher compression ratio (29 kW instead of 30 kW). All values were measured on a stationary engine test bench and could be reproduced. Intake air temperature and pressure, coolant and oil temperatures were controlled to be in the same order of magnitude when comparing identical operating points for both engines. The engine specifications are presented in Table 2. The efficiency curves were determined from a fuel consumption map for all measured operating points (more than 100 measurements for each engine). For a given power hyperbola, the point with the best brake efficiency of the advance engine was found. It is given in Fig. 2. As an outlook, further potential of the combustion

engine could be exploited by the usage of direct injection (DI), possibly in conjunction with alternative fuels. DI can contribute to an increase in thermodynamic efficiency at higher loads compared to PFI, because of earlier spark timing, which leads to a heat release closer to ideal combustion. Alternative fuels, such as ethanol or gasoline/ethanol blends are less knock restricted than conventional RON95 gasoline fuel and can enforce this effect. As a result, higher efficiency and even higher power output for stoichiometric operation could be achieved.

Table 2: Engine specifications

	Baseline	Advanced
EGR	Internal	External
Compression ratio increase	+0	+1
Peak power	30 kW	29 kW
Exhaust manifold	Conventional	Integrated into cylinder head
Displacement	1.0 l	1.0 l
Valvetrain	Intake camphasing	Intake camphasing

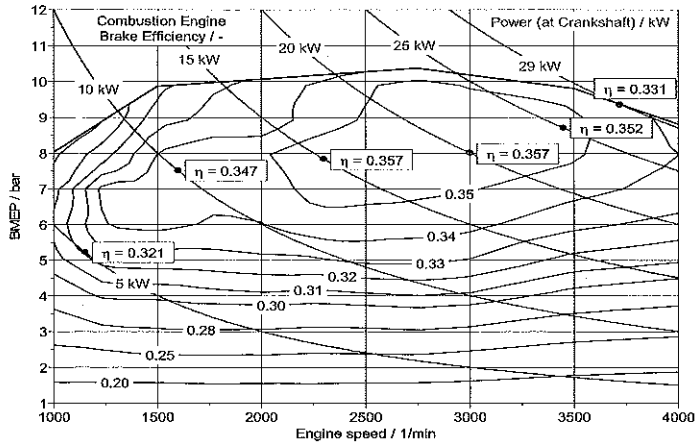

Figure 2: Brake efficiency of the advanced engine

C. Transmission

The transmission used for the high speed concept consists of one planetary gear stage with a gear ratio of -4.6. The high speed side is connected to the electrical machine. The

transmission was employed for a high speed electrical drive for mobile machinery [5]. It can also be applied to this REX concept since the required torque-speed characteristics are similar. The transmissions' architecture is advantageous for high rotational speeds. Due to the fixed planet carrier no centrifugal loads act upon the planet bearing and no paddling losses of the carrier occur. In order to achieve a high running smoothness, a helical gearing is chosen. For all shafts (sun, ring and planet) roller bearings are applied. For the dynamic sealing locations, radial shaft seals are used. The transmission's characteristics are listed in Table 4. For the simulation, a measured efficiency map of the high speed transmission is used. The efficiency map is scaled from 20 kW (application: mobile machinery) to 30 kW (application: REX). The surrogate model of the scaled efficiency map was built based on a stochastic process model for estimation of un-experimented points. The details of the stochastic process model can be found in [6]. All losses of gear meshing, bearings, seals and the injection lubrication are included. Therefore the transmission's efficiency is both load and speed dependent. Efficiency reaches 98.1 % in the full load range at moderate speeds (5 000 rpm) and 96.2 % at high speeds and full load (20 000 rpm). Figure 3 shows the efficiency map of the transmission.

Table 3: Transmission characteristics.

max. torque (electrical motor side)	95 Nm
max. rotational speed (electrical motor side)	20 000 rpm
power	20 kW
gear ratio	-4.6
weight	21.6

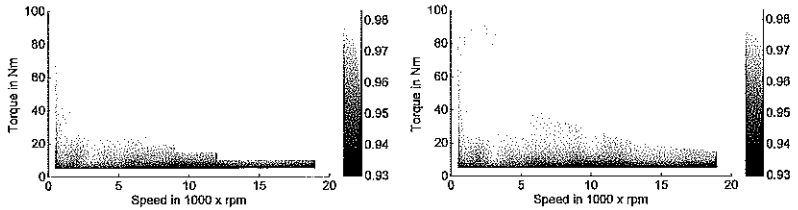

Figure 3: Efficiency map of the transmission obtained from (a) experiments (b) surrogate model.

D. Generators

1) Direct-driven permanent magnet generator

The electric machine described in [7] is employed for the REX application. The efficiency map has been built by finite element analysis (FEA), including mechanical losses, as shown in Fig. 4. An additional constant efficiency of 97 % is applied to the efficiency map in consideration of the inverter.

Table 4: Main dimensions and weight of two generators.

	Direct driven	Gear driven
Generator specifications		
Rated power	30 kW@base 2860 rpm	30 kW@base 12k rpm
Rotor diameter (mm)	113	70
Stator diameter (mm)	204	135
Stack length (mm)	80	141
Slots/poles	36/6	36/4
DC link voltage (V)	400	400
Generator active material weight		
Iron core (kg)	13.4	10.6
Permanent magnet (kg)	0.67	0.52
Copper (kg)	6.83	2.35
Generator system weight		
Gear-box (kg)	-	21.6
Generator system total mass (Incl. Power module)	46.1 kg	50.6 kg

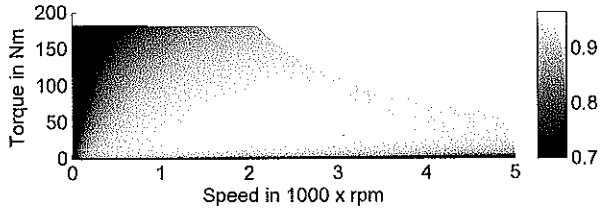

Figure 4: Efficiency map of the direct driven generator.

2) Gear driven permanent magnet generator

The speed of the generator with the single stage transmission described in the section above is 4.6 times faster than the direct-driven generator. Therefore, a reduction in total weight and

costs can be expected. The generator is analyzed by the operating conditions given by the engine and transmission. Table 4 present the dimension and parameters of both generators.

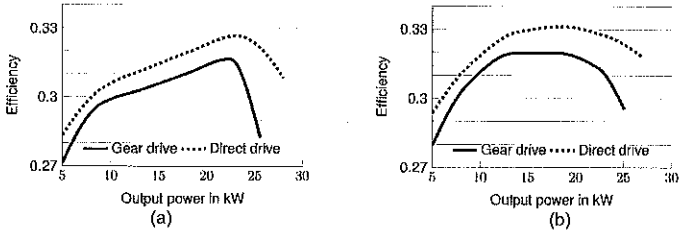

Figure 5: Combined efficiency of generators with (a) the base (b) the advanced engine.

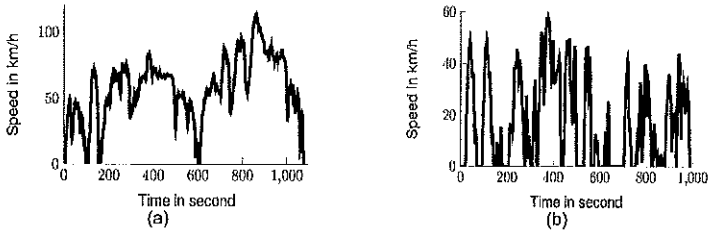

Figure 6: Speed profile of Artemis driving cycle (a) Rural (b) Urban.

3. Driving cycle simulation with a power management controller

The output power of REX has to be controlled and determined since the REX-EV has two power source: REX and battery. The algorithm employed in this study for the power management control of the vehicle is the model predictive control [8]. The minor implementations for on and off conditions are given. The REX operates only at its most efficient speeds and loads as it is not coupled to the wheels. Therefore, the REX efficiency of each component can be combined to form the efficiency curve, which is a function of the REX output power. The combined efficiency of the engine, generator and transmission, in case of the gear driven, used in the simulation is shown in Fig. 5 for each topology. The consumed fuel on each driving cycle can be calculated as

$$m_f = \frac{\int_{t_0}^{t_{end}} P_e(t)\cdot dt}{H_u \eta_{rex}}. \qquad (7)$$

Figure 6 depicts Artemis urban and rural driving cycle which is used in the simulation. The Artemis cycles are chassis dynamometers based on statistical analysis of a large database of European real world driving patterns [9]. The complete simulation architecture of this paper is illustrated in Fig. 7. As the SOC of each topology is different at the end of driving,

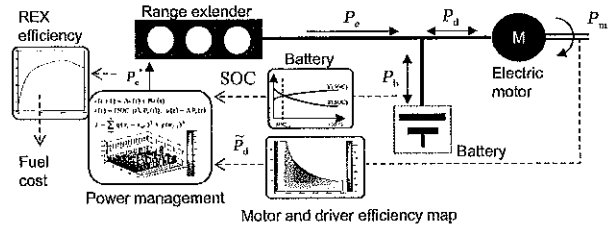

Figure 7: Schematic representation of a REX-EV with a power management controller.

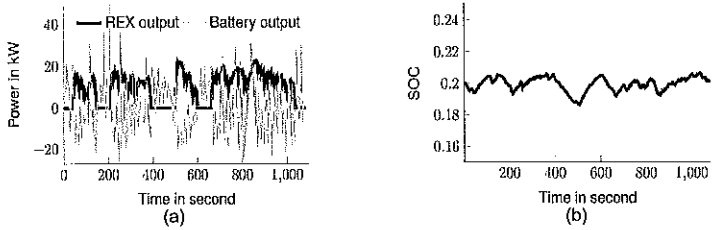

Figure 8: Simulation results on Rural driving cycle (a) Output power profile (b) SOC.

the following condition can be established for a fair comparison in charge depleting mode:

$$SOC_{end} = SOC_{start} . \quad (8)$$

The net energy usage of the battery has to be zero in the charge depleting mode:

$$\int_{t_0}^{t_{end}} (n_{ch}(t) P_b^+(t) + \frac{P_b^-(t)}{n_{dis}(t)}) dt = 0 , \quad (9)$$

where the positive and negative upper script is a charging and discharging notation respectively. The additional fuel corresponding following condition is added to (7):

$$m_f' = \frac{1}{H_u \bar{n}_e^+} \int_{t_0}^{t_{end}} \left(n_{ch}(t) P_b^+(t) + \frac{P_b^-(t)}{n_{dis}(t)} \right) dt. \quad (10)$$

$\bar{n}_e^+$ is average efficiency of REX, when the battery is charged by the REX. The combination of (7) and (10) resolves the consumed fuel in different SOC conditions at the end of driving. The vehicle parameters in Table 1 are used for this simulation. All topologies are simulated with the same control parameters but different reference output power. Therefore, the efficiency of such reference power is the highest over all possible operating points.

The simulation was performed on three different Artemis cycles with 800 W auxiliary power consumption. The results are given in Table 5 and Table 6 for the topologies with the advanced and the baseline engine respectively. The required acceleration under -1.2 m/s² to follow the driving cycle is assumed as mechanical braking instead of regenerative braking.

Table 5: Fuel economy and efficiency of two generators with the advanced engine.

	Advanced					
	Direct driven			Gear driven		
	Urban	Rural	Motorway	Urban	Rural	Motorway
Fuel consumption (kg)	0.27	0.69	1.60	0.28	0.71	1.77
Fuel economy (km/l)	15.05	20.79	14.96	14.69	20.21	13.56
Average REX efficiency	31.8 %	32.4 %	32.1 %	31.1 %	31.6 %	29.5 %

Table 6: Fuel economy and efficiency of two generators with the baseline engine.

	Baseline					
	Direct driven			Gear driven		
	Urban	Rural	Motorway	Urban	Rural	Motorway
Fuel consumption (kg)	0.28	0.72	1.63	0.29	0.74	1.78
Fuel economy (km/l)	14.52	20.09	14.70	14.05	19.57	13.50
Average REX efficiency	31.0 %	31.3 %	31.5 %	30.0 %	30.5 %	29.2 %

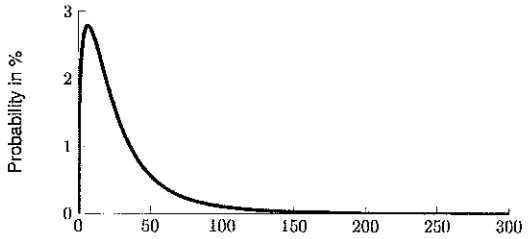

Figure 9: Probability distribution of daily travel distance.

Therefore, the demand power is zero during the time period. The allowable maximum charging power of the battery is set to 40 kW. The output power profile and the SOC of the battery on Artemis rural cycle are shown in Fig. 8. The daily driving cost can be calculated based on the previous simulation results. The additional weighting factor, in consideration of the total trip number percentages in [9], is used for the calculation of the average daily driving costs as follows:

$$C_f = \sum_{i=1}^{3} c_i \cdot w_i \quad (11)$$

Table 7: Daily driving costs of each topology.

	Baseline		Advanced	
	Direct driven	Gear driven	Direct driven	Gear driven
Electricity cost (Euro/kWh)	0.3		0.3	
Fuel cost (Euro/ℓ)	1.49		1.49	
Weighted fuel economy(km/ℓ)	16.08	15.56	16.64	16.19
Daily driving cost (Euro)	3.89	3.98	3.80	3.87

Table 8: Estimated cost of generator systems.

	Direct driven	Gear driven
Generator active material cost (Euro)	174	115
Generator construction (Euro)	100	100
Power module (Euro)	180	180
Auxiliary system cost (Euro)	150	150
Gear box (Euro)	-	1200
Total (Euro)	604	1745

, where c_i is each driving cost per km and w_i is the weighting factor which is 0.697, 0.275, 0.029 for the urban, rural, and motorway cycle respectively. Figure 9 depicts the density of the daily driving distance of the family car obtained from NHTS survey [10]. The expected daily driving cost can be calculated, using the previous probability, as

$$\text{Expected cost} = C_e \int_0^{D_e} xp(x)\mathrm{d}x + C_f \int_{D_e}^{D_{fin}} xp(x)\mathrm{d}x, \tag{12}$$

where C_e is the electricity costs per km, C_f is the fuel costs per km and D_e is the electrical driving distance respectively. The electrical driving distance is calculated as 79 km (0.17 kWh/km) and D_{fin} is chosen as 800 km. The calculated driving costs and the parameters are given in Table 7.

4. Comparison and discussion

The significant advantages of the gear driven generator over direct driven generator cannot be found. The portion of the gear mass is heavier than the reduced mass of the gear driven generator when compared to the direct driven generator which leads to nearly the same mass. The estimated system costs for the direct driven and the gear driven topologies are compared in Table 8. The reduced costs of the gear driven generator cannot lead to positive results due to the costs of the transmission. The general reason is that the output power of the generator for this application is not high to give a significant reduction of the costs by the reduced material utilization of the generator. The most expensive material of the generator is a permanent magnet which is 25 Euro (48 Euro/kg) for the active material costs of the gear driven generator. The cost reduction by a high speed generator is not expected in the REX of family car size application even for a permanent magnet-less generator. In addition, mechanical losses in the transmission lead to worse efficiency of the gear driven generator. As the well-matched gear ratio can increase the combined efficiency of the generator and engine [3], the dedicated design of a direct driven generator for one specific engine can be expected to show good performance. The driving costs of each topology do not differ much. Since the REX-EV is pure electrically driven over the average daily driving distance of family cars (53 km [10]), the probability of driving further distances is not high. This leads to the small differences of the driving costs in charge depleting mode.

5. Conclusion

The numerical simulation results for direct driven generator and gear driven generator have been compared with two different engines. The fuel efficiency of each topology was obtained by the driving cycle simulation with combined efficiency of the generator, gear and engine, assuming that the REX is operated at most efficient loads and speed. For both engines, the direct driven REXs showed better efficiency due to the removed gear stage. The difference of mass between direct driven and gear driven topologies was 4.5 kg, which is a negligible difference. Due to the costs of the transmission, the system costs of the gear driven generator were higher compared to the direct driven generator. The reduced costs of the gear driven generators were dominated by the cost of transmission. The driving cost analysis showed that the estimated cost differed only slightly between two topologies. As the battery capacity (15 kWh) is enough to cover the average daily driving distance, which is 53 km, the probability of consuming fuel is not high. The analysis results based on the NHTS survey differed only 0.17 Euro in cost differences between the best and worst variant. The cost effective and light REX is revealed as a suitable REX for a family car application under the given NHTS survey data.

6. Acknowledgements

The authors would also like to thank the "Deutsche Forschungsgemeinschaft (DFG)" for the funding of the graduate school 1856 „Integrated Energy Supply Modules for On-Road Electro mobility".

Reference

[1] C.-F. Wang, M.-J. Jin, J.-X. Shen, and C. Yuan, "A permanent magnet integrated starter generator for electric vehicle onboard range extender application," IEEE Trans. Magn. , vol. 48, no. 4, pp. 1625–1628, Apr. 2012.

[2] Y.-k.Kim, S.Salvi, A.G. Stefanopoulou, and T. Ersal "Reducing Soot Emissions in a Diesel Series Hybrid Electric Vehicle Using a Power Rate Constraint Map," IEEE Trans. Vehicular Technology, vol. 64, no.1, pp.2-12, 2015.

[3] M.-j.Kim, D.-b. Jung, and K.-d.Min, "Hybrid Thermostat Strategy for Enhancing Fuel Economy of Series Hybrid Intracity Bus," IEEE Trans. Vehicular Technology, vol 63, no. 8, pp. 3569-3579, 2014.

[4] V. Sezer, M. Gokasan, and S. Bogosyan, "A novel ECMS and combined cost map approach for high-efficiency series hybrid electric vehicles," IEEE Trans. Veh. Technol., vol. 60, no. 8, pp. 3557–3570, Oct. 2011.

[5] J. Schröter, G. Jacobs, "High Speed Electrical Drives for Mobile Machinery – Drive Concept and Selected Components," 13th International CTI Symposium, Berlin, Germany, December 8th – 11th, 2014.

[6] E. Rasmussen and C. K. I. Williams, "Gaussian Processes for Machine Learning, Cambridge, MA: MIT Press," 2005.

[7] G. Ripaccioli, D. Bernardini, S. Di Cairano, A. Bemporad, and I. Kolmanovsky, "A stochastic model predictive control approach for series hybrid electric vehicle power management," American Control Conference (ACC). IEEE, 2010, pp. 5844–5849.

[8] T. Grosse, K. Hameyer, and J. Hagedorn, "Needle winding technology for symmetric distributed windings," EDPC 2014, Nuremberg, Germany, 30. Sept – 1. Oct, 2014.

[9] André, Michel, "The ARTEMIS European driving cycles for measuring car pollutant emissions," Science of the total Environment 334 (2004), pp73-84.

[10] National Household Travel Survey ; Available from: http://nhts.ornl.gov/. (Retrieved Sept. 2015).